

Chemical Fingerprinting–Driven Insights into the Pharmacobotany and Bioactivities of *Cymbopogon Citratus* (DC.) Stapf

S.A. Wasim Akram^{1*}, J. John Christopher¹, Mary Shamy Arokia Rajan¹, S. Mageswari¹, S. Tirumala Santhosh Kumar¹, K. Kabiruddin¹

¹Regional Research Institute of Unani Medicine, No-1, West Mada Church Road, Royapuram, Chennai – 600 013, Tamil Nadu, India

DOI: <https://doi.org/10.36348/sijtem.2025.v08i10.004>

| Received: 26.09.2025 | Accepted: 22.11.2025 | Published: 24.11.2025

*Corresponding author: S.A. Wasim Akram

Senior Research Fellow (Botany), Regional Research Institute of Unani Medicine, No-1, West Mada Church Road, Royapuram, Chennai – 600 013, Tamil Nadu, India

Abstract

Cymbopogon citratus (DC.) Stapf. (lemongrass) is a widely used medicinal grass valued for its essential oils and diverse therapeutic properties; however, comprehensive pharmacogenetic documentation of the whole plant remains limited. The present study provides an integrated evaluation of the pharmacobotanical, antimicrobial, antioxidant, and chemical fingerprinting characteristics of *C. citratus* collected from the northeast coast of Tamil Nadu, India. Macroscopic and microscopic analyses established diagnostic features including sclerenchymatous vascular bundle sheaths, bulliform cells, dumb-bell-shaped silica bodies, prickly hairs, and annular vessels, providing robust anatomical markers for authentication. Physicochemical parameters (LOD, ash values, extractive values, pH) confirmed good-quality raw material with minimal foreign matter. The hydro-alcoholic whole-plant extract exhibited broad-spectrum antimicrobial activity, with pronounced inhibition against *Staphylococcus aureus* and *Enterococcus faecalis*. Potent antioxidant activity was recorded in the DPPH assay, with an IC₅₀ of 39.37 µg/mL, attributed to phenolic and flavonoid constituents. HPTLC profiling generated a reproducible chromatographic fingerprint with recurring marker bands at R_f 0.08, 0.04, and 0.01 under 254 nm and 366 nm, reflecting the chemical diversity of the extract. This study provides the first complete pharmacogenetic framework for *C. citratus* whole plant, offering essential baseline data for authentication, standardization, and future phytopharmaceutical development. Further studies on quantitative marker estimation, MIC/MBC analysis, and bioactivity-guided fractionation are recommended to strengthen its therapeutic applicability.

Keywords: *Cymbopogon citratus*; Pharmacognosy; Antimicrobial activity; Antioxidant activity; HPTLC fingerprinting.

Copyright © 2025 The Author(s): This is an open-access article distributed under the terms of the Creative Commons Attribution 4.0 International License (CC BY-NC 4.0) which permits unrestricted use, distribution, and reproduction in any medium for non-commercial use provided the original author and source are credited.

INTRODUCTION

Medicinal plants have been widely used since ancient times and continue to play a significant role in global healthcare systems. According to the WHO, a large portion of the population in developing countries still relies on plant-based traditional medicine for primary healthcare needs [1]. In regions across Africa and Asia, herbal remedies remain deeply rooted in cultural practices and are used for treating various ailments [2]. Globally, more than 25,000 plant species are estimated to possess medicinal value, and their pharmacological properties are continually being explored through modern scientific approaches [3]. Recent advances in ethnopharmacology and phytochemistry have strengthened the understanding of medicinal plants by revealing the significance of complex phytochemical mixtures rather than single isolated compounds [4]. These synergistic interactions

among bioactive metabolites contribute to enhanced therapeutic efficacy compared to conventional single-drug treatments [5].

The family Poaceae includes herbaceous and perennial grasses with diverse morphological characteristics, such as erect or prostrate stems and distichous leaves composed of a sheath, ligule, and lamina [6]. Within this family, *Cymbopogon* is a widely distributed genus in tropical and subtropical regions of Africa, Asia, and the Americas, comprising approximately 144 species renowned for their essential oil content [7]. Essential oils from *Cymbopogon* species are rich in phytochemicals, including limonene, citral, elemol, citronellal, 1,8-cineole, linalool, geraniol, and β-caryophyllene [8]. The antioxidant properties of medicinal plants are largely attributable to these secondary metabolites, particularly phenolics,

flavonoids, tannins, terpenoids, carotenoids, and lignans [9].

Cymbopogon citratus (lemongrass) grows well in a variety of soil types but prefers well-drained sandy loam soil under high sunlight [10]. Known for its characteristic lemon aroma, it has extensive use in perfumery, cosmetics, culinary preparations, and beverages [11]. In traditional medicine, leaf decoctions are used as diaphoretics and remedies for fever [12]. Pharmacological studies have reported diverse bioactivities, including digestive stimulation, modulation of xenobiotic-metabolizing enzymes, and potential chemopreventive effects [13].

In Ayurveda, *C. citratus* is valued for its tranquilizing, diuretic, antipyretic, and anti-inflammatory properties [14]. Its essential oils, particularly citral, exhibit notable antifungal activity against *Candida* spp. [15]. Additionally, phenolic and flavonoid components contribute to its potent antioxidant capacity, while various extracts have demonstrated antiprotozoal, anticarcinogenic, cardioprotective, antitussive, antiseptic, and antirheumatic effects [16]. Compounds such as citral, myrcene, and citronellal have also shown significant antimalarial activity in vitro against *Plasmodium* spp. and may enhance antioxidant defenses during malaria-associated oxidative stress [17 & 18].

Despite the extensive traditional and pharmacological relevance of *Cymbopogon citratus*, comprehensive pharmacognostical documentation of the whole plant remains limited. Most existing studies focus primarily on essential oils or isolated phytochemicals, overlooking the need for standardized morphological, microscopic, physicochemical, and chromatographic parameters essential for reliable quality control. This study fills these gaps by providing an integrated pharmacognostic profile, including macroscopy, microscopy, physicochemical constants, antimicrobial and antioxidant evaluation, and a detailed HPTLC fingerprint. The findings offer essential baseline data for authentication, standardization, and future formulation development, thereby strengthening the scientific foundation and therapeutic credibility of *C. citratus*.

MATERIALS AND METHODS

Collection of Plant Material

Whole plants of *Cymbopogon citratus* (DC.) Stapf were collected from Varadharaja Nagar, Chengalpattu, Tamil Nadu, India (Latitude 12.677029°; Longitude 79.978523°). The specimen was authenticated by Dr. K. Venkatesan, Assistant Research Officer (Botany), Survey of Medicinal Plants Unit, and a voucher specimen (No. 1522) was deposited for future reference. The plant was separated into leaves, stems, and roots, which were shade-dried at room temperature for 15–20 days. Dried materials were pulverized into coarse powder and stored in airtight containers.

Pharmacognostical analyses were performed on fresh leaf, stem, and root samples.

Pharmacognostical Studies

Pharmacognostical parameters were examined using the standard procedures recommended by the Pharmacopoeia Commission for Indian Medicine and Homoeopathy (PCIM&H), Ministry of AYUSH, Government of India. Macroscopic, microscopic, and powder microscopy studies followed the methods described by [19]. Fresh transverse sections of leaf, stem, and root were prepared, stained with safranin, and mounted in glycerine for microscopic observation. Powder studies involved treatment with diagnostic reagents such as phloroglucinol-HCl and Jefferey's reagent to visualize structural components [20]. Photomicrographs were captured at various magnifications using a Nikon Eclipse Ci microscope.

Physicochemical Analysis

Physicochemical parameters, including loss on drying (LOD), extractive values (alcohol, hexane, and water), total ash, acid-insoluble ash, pH, and volatile oil content, were determined according to WHO and API standard methods [21].

Antimicrobial Activity

Preparation of Extract

One hundred grams of dried whole-plant material was extracted twice with 400 mL of 70% (v/v) hydro-alcohol for 48 hours at room temperature. Filtration was carried out using Whatman No. 1 filter paper, and the filtrate was concentrated using a rotary vacuum evaporator at 50°C. The resulting semisolid extract was dissolved in 10% dimethyl sulfoxide (DMSO) to obtain a stock concentration of 100 mg/mL.

Inoculum Preparation

Bacterial strains *Staphylococcus aureus* (ATCC 29213), *Enterococcus faecalis* (ATCC 29212), *Klebsiella pneumoniae* (ATCC 700603), *Escherichia coli* (ATCC 25922), and the fungal strain *Candida albicans* (clinical isolate, Cochin University) were procured from the Centre for Drug Discovery and Development, Sathyabama Institute of Science and Technology, Chennai. Isolates were cultured on Mueller-Hinton agar (MHA) and *C. albicans* on Sabouraud Dextrose agar (SDA) for 24 h at 37°C. A single colony was inoculated into Mueller-Hinton broth or Sabouraud broth and incubated overnight at 37°C with shaking (200 rpm). Cell suspensions were adjusted to approximately 1×10^8 CFU/mL, corresponding to 0.5 McFarland standard.

Disc Diffusion Assay

Antimicrobial efficacy of the hydro-alcoholic extract was assessed using the standard disc diffusion method according to CLSI guidelines [22]. Sterile cotton swabs were used to lawn microbial suspensions on MHA (bacteria) and SDA (fungi). Sterile 6-mm discs were

impregnated with 10 μ L of extract at concentrations of 10 mg/mL and 25 mg/mL. A negative control (10% DMSO) and standard reference drug were included. Plates were incubated at 37°C for 12–24 h, and the diameter of the inhibition zone (including the disc) was measured in millimeters.

Antioxidant Activity

DPPH Radical Scavenging Assay

The antioxidant activity of the whole-plant extract was evaluated using the 2,2-diphenyl-1-picrylhydrazyl (DPPH) assay described [23], with minor modifications. In a 96-well plate, 100 μ L of 0.1 mM DPPH in methanol was mixed with 100 μ L of extract at concentrations of 50, 100, 250, and 500 μ g/mL prepared from a 50 mg/mL stock. L-ascorbic acid served as the positive control, and respective blanks were included. Plates were kept in the dark for 30 minutes, and absorbance was recorded at 517 nm using an ELISA reader Robonik.

Percentage inhibition was calculated as: %Inhibition = $(A_0 - A_1/A_0) \times 100$

Where: A_0 : absorbance of control; A_1 : absorbance of sample

Sample Preparation for HPTLC

Two grams of coarse whole-plant powder was macerated in 20 mL of alcohol overnight, filtered through Whatman No. 1 filter paper, and stored for analysis.

Chromatographic Conditions (HPTLC)

HPTLC analysis was performed on 10 \times 10 cm precoated silica gel 60 F₂₅₄ plates (E. Merck, Germany). Samples were applied as 8-mm bands using a CAMAG Automatic TLC Sampler IV equipped with a 100 μ L syringe. A twin-trough chamber was saturated with mobile phase (toluene:ethyl acetate:formic acid, 8.4:1.6:0.01) for 15 min at ambient temperature. The chromatographic run length was 80 mm. Plates were scanned with a CAMAG TLC Scanner 4 at 254 nm and 366 nm in absorbance and fluorescence modes. Visualization was performed using the CAMAG TLC Visualizer. Data acquisition and analysis were carried out using WinCATS version 1.4.9.2001. Nitrogen served as the carrier gas under high-pressure conditions. Deuterium-tungsten and mercury lamps were used for absorbance measurements at 254 nm and 366 nm.

Statistical Analysis

All experiments were performed in triplicate ($n = 3$). Data were expressed as mean \pm standard deviation (SD). Statistical analyses were conducted using SPSS version 20.0 (IBM Corp., USA). Group differences were assessed using one-way analysis of variance (ANOVA), followed by Tukey's post hoc test. A p -value < 0.05 was considered statistically significant.

RESULT

Pharmacogenetic Studies

Macroscopic Features



Fig. 1: Morphological attributes of *C. citratus*. a. Habit; b. Whole Plant-surface view; c. Root-surface view

The whole plant of *Cymbopogon citratus* exhibits characteristic grass-like morphology. The root system consists of fibrous, short, woody stumps that give rise to numerous culms—typical features reported in recent Poaceae anatomical descriptions (Sharma *et al.*, 2021). The culm is erect, terete, smooth, and shiny, with

solid internodes measuring 5–16 cm. Leaves are linear-lanceolate (up to 50 cm \times 3.5 cm), tapering into a filiform apex, with a glabrous surface and scabrid margins. The midrib is prominently raised on the abaxial surface. Leaf sheaths are shorter than the internodes, tightly clasping the culm, and bear membranous ligules (2–3 cm). The

inflorescence is a compound spathe-type panicle (up to 30 cm), with paired racemes and characteristic sessile and pedicellate spikelets, similar to previously reported *Cymbopogon* species (Bashir *et al.*, 2022). **Fig.1**

Microscopic Features

Root

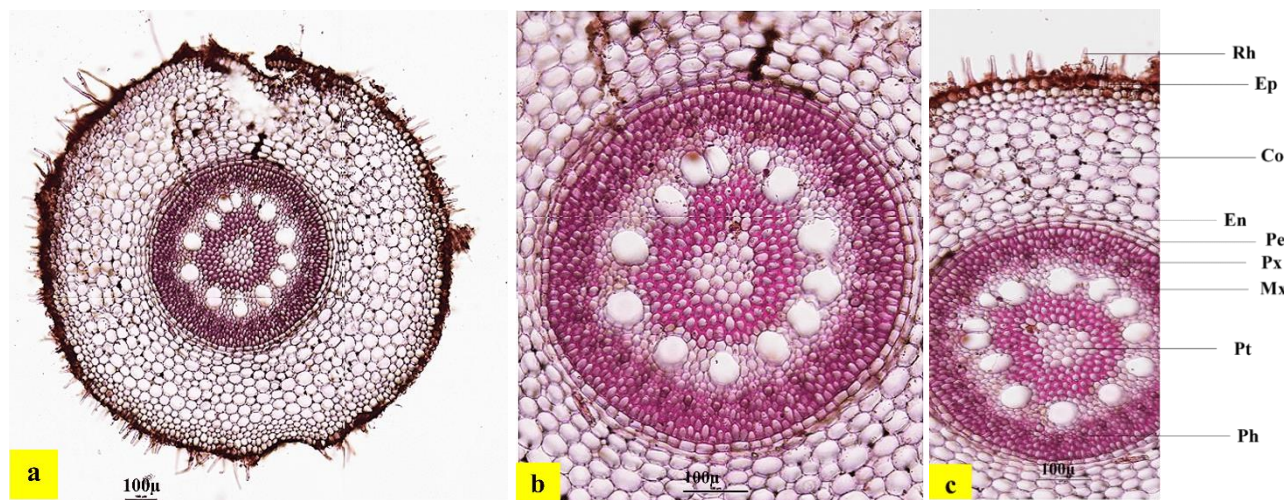


Fig. 2 Anatomical features of *C.citratus*: a. T.S. of Root; b. Central portion; c. A portion Enlarged Rh-Root hair; Ep-Epidermis; Co-Cortex; En-Endodermis; Pe-Pericycle; Px-Protoxylem; Mx- Metaxylem; Pt-Pith; Ph- Phloem

Transverse section (T.S.) of the root shows a circular outline with a uniseriate epidermis bearing unicellular root hairs. The cortex consists of thin-walled parenchyma with large air cavities. The endodermis forms the innermost continuous layer, followed by a sclerenchymatous pericycle. Vascular bundles are radial, with metaxylem vessels centrally placed and protoxylem

towards the periphery—features consistent with monocot medicinal grasses (Sharma *et al.*, 2021). The pith is small and composed of thick-walled parenchyma.

Fig.2

Stem

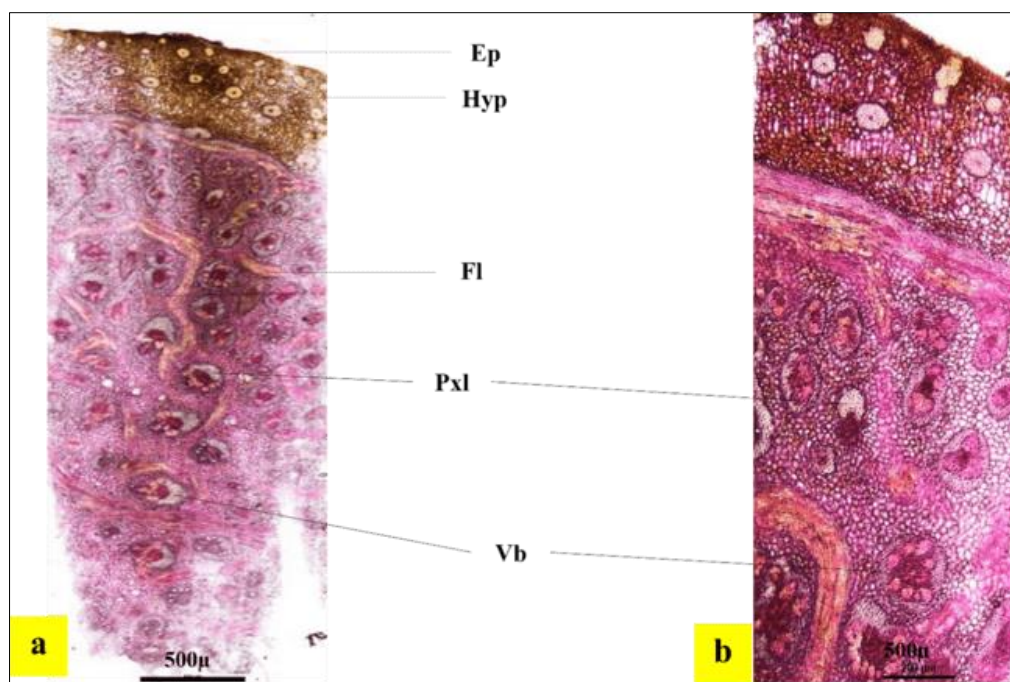


Fig. 3: Anatomical features of *C.citratus*; a. T.S. of Stem; b. A portion enlarged Ep-Epidermis; Hyp-Hypodermis (Sclerenchyma and Collenchyma cells); Fl-Fibrous layer; Pxl-Protoxylem lacuna; Nvb-Numerous vascular bundles;

T.S. of the stem is circular with a thick cuticularized epidermis. The hypodermis includes patches of sclerenchyma over parenchymatous tissue. A fibrous ring is present above the parenchymatous ground tissue. Numerous collateral, closed vascular bundles with sclerenchyma sheaths are scattered throughout the

ground region, in agreement with the structural descriptions of *C. citratus* reported by Almarzuqi *et al.*, (2023). **Fig.3**

Leaf (Midrib and Lamina)

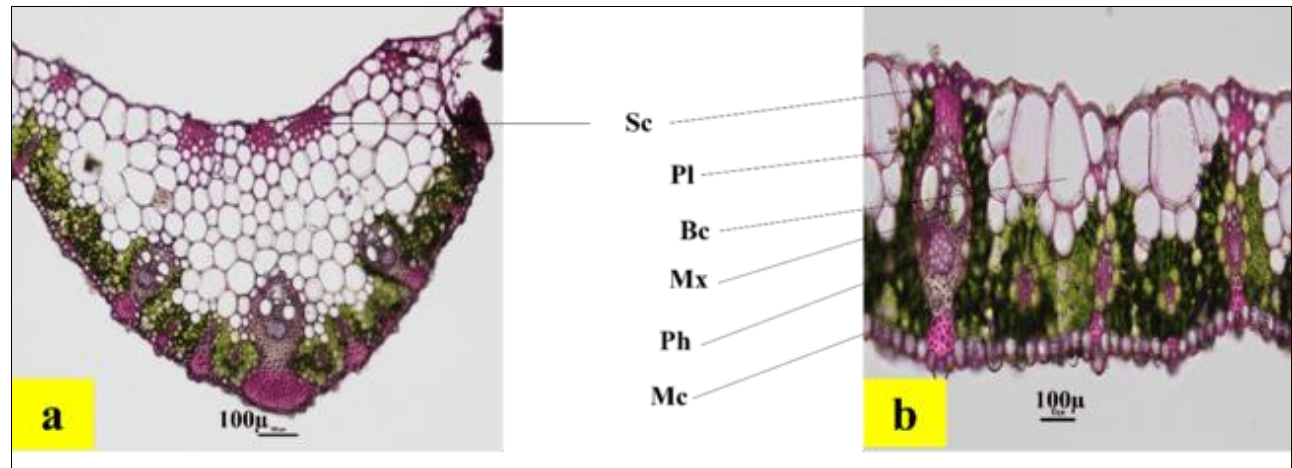
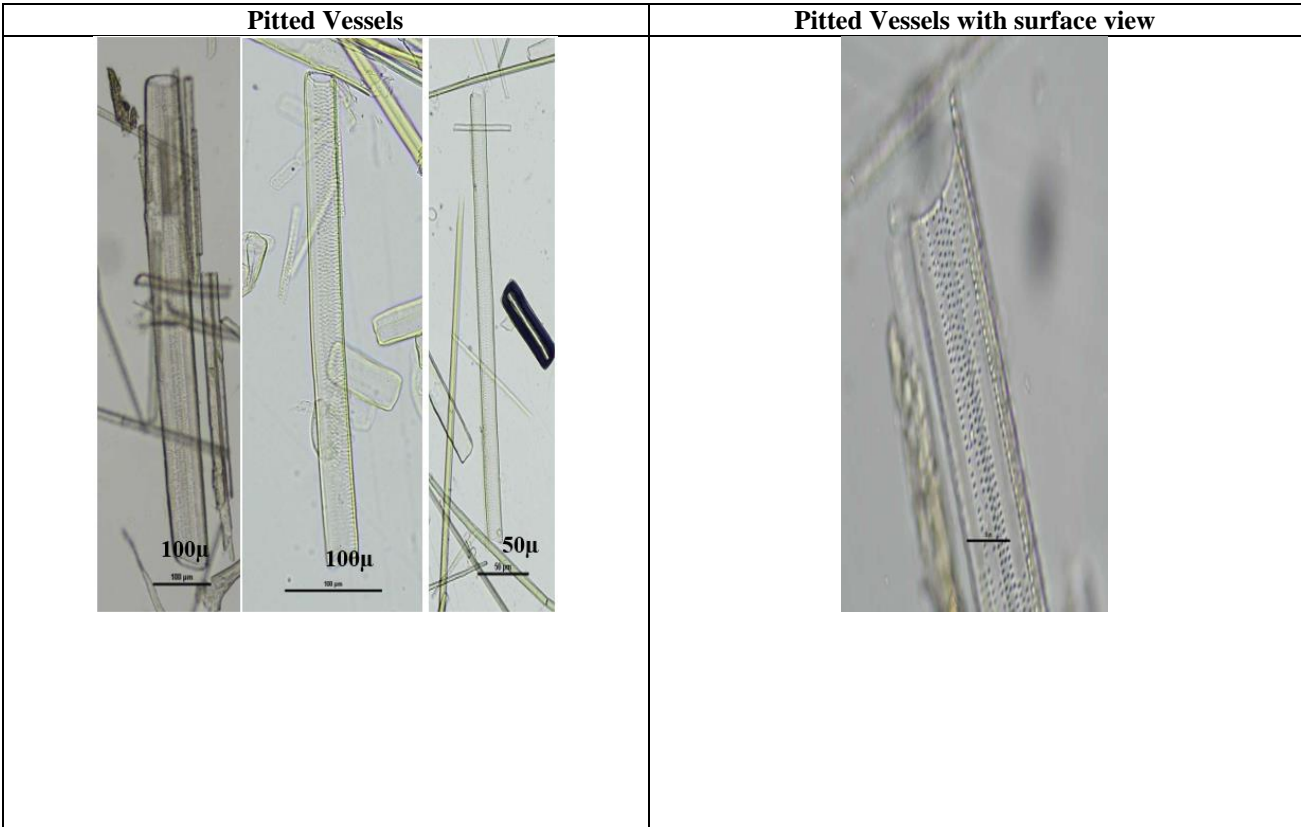


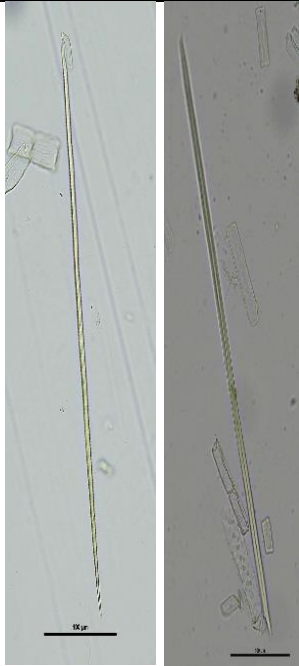
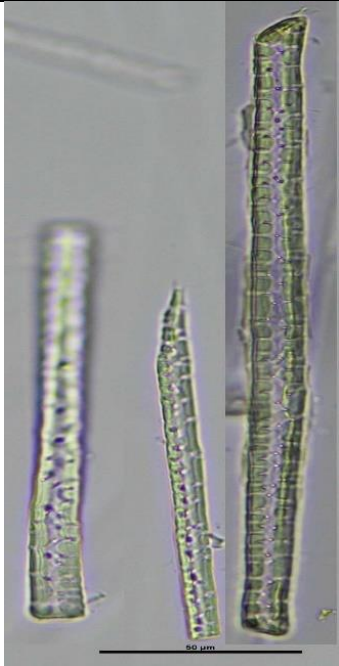
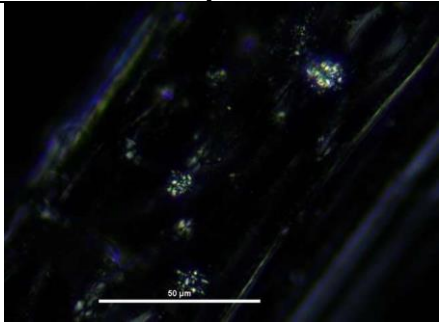
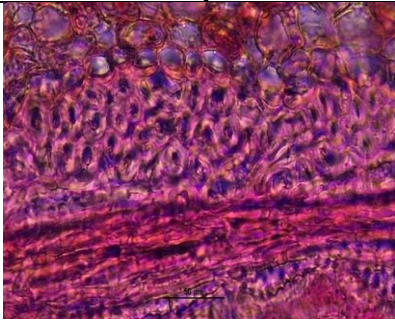
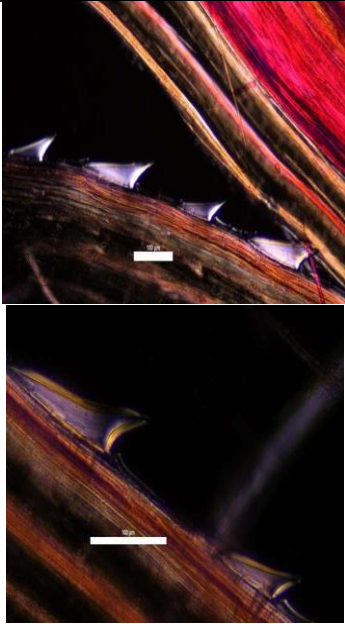
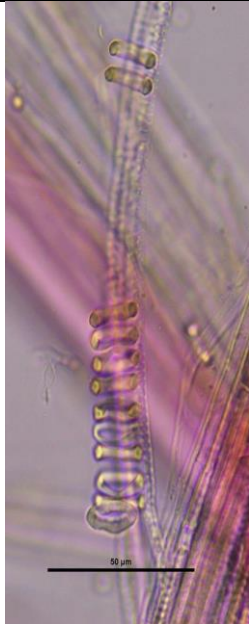
Fig. 4: Anatomical features of *C.citratus*; a. T.S. of Midrib; b. T.S. of Lamina Sc-Sclerenchyma cells; Pl-Protoxylem Lacuna; Bc-Bulliform cells; Mx-Metaxylem; Ph-Phloem; Mc-Mesophyll cells;

The leaf is isobilateral. The adaxial surface is concave, with bulliform cells interrupting the epidermis. Both surfaces bear stomata arranged between parallel veins. Mesophyll is spongy, consisting of 4–6 layers of parenchyma. Vascular bundles diminish in size towards the margin and are surrounded by sclerenchyma sheaths.

Metaxylem vessels are conspicuous. The lamina shows dumb-bell-shaped silica bodies, microhairs, papillae, and prickles—well documented diagnostic features of *Cymbopogon* species (De Carvalho *et al.*, 2023). **Fig.4**

Powder Characteristics



<p>Fibres</p> 	<p>Elongated sclereid like cells</p> 
<p>Crystals</p> 	<p>Sclerenchyma cells</p> 
<p>Trichomes</p> 	<p>Annular Vessels</p> 

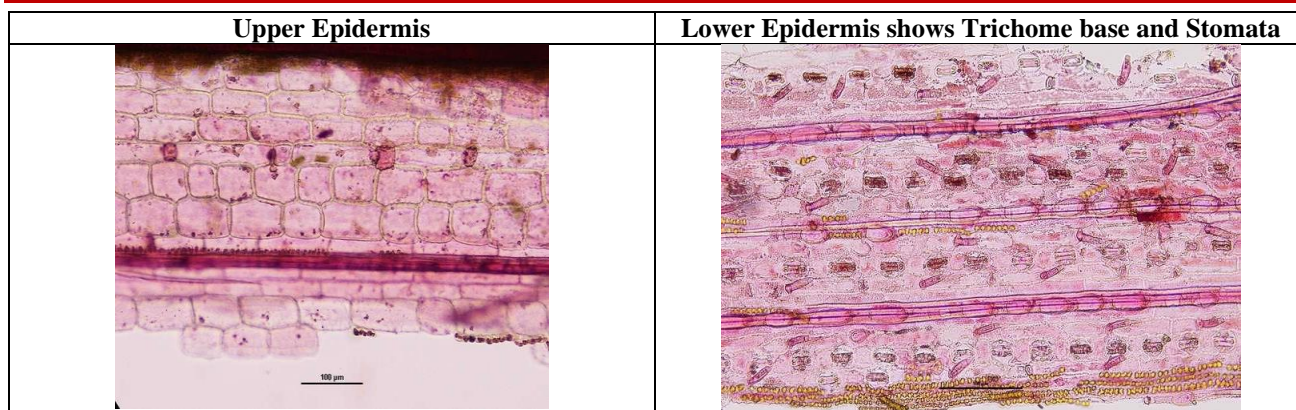


Fig. 5: Powder features of *C.citratus* – Whole plant

Powdered plant material is brown and fibrous. Diagnostic microscopic characters include: graminaceous stomata, pitted vessels (up to 50 µm), crystals (up to 15 µm), thick-walled sclereids (up to 175 µm × 20 µm), fibres (600 µm × 15 µm), sharp-tipped trichomes (≈200 µm), annular vessels (≈20 µm), and

elongated parenchyma cells. Similar diagnostic markers were reported by Moghadamtousi *et al.*, (2021) for *Cymbopogon* species. **Fig. 5**

Physico-Chemical Parameters

Table 1: Physico-chemical constants of *C.citratus* Whole plant

S. No	Parameters	Values (%)
1.	Foreign matter	0.01%
2.	LOD	7.32%
3.	Total ash	5.62%
4.	Acid-insoluble ash	5.10%
5.	Alcohol soluble extractives	5.30%
6.	Hexane soluble extractives	0.59%
7.	Water soluble extractives	5.24%
8.	pH	7.2

Physicochemical constants including loss on drying, ash values, extractive values, and pH are summarized in **Table 1**. The relatively low foreign matter (0.01%) and pH of 7.2 indicate good sample quality. Total ash (5.62%) and acid-insoluble ash (5.10%) reflect the mineral and silica content typical of

Poaceae plants (Nunes *et al.*, 2020). Extractive values demonstrate good solubility of constituents in alcohol (5.30%) and water (5.24%).

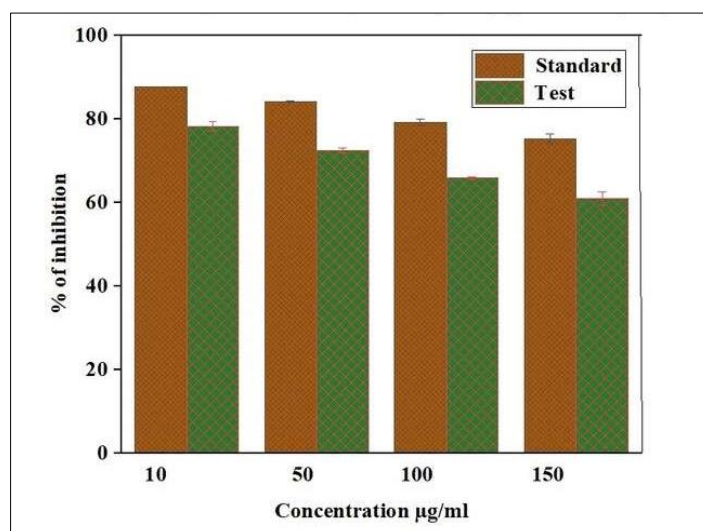
Antimicrobial Activity

Table 2: Antimicrobial screening test of whole plant extract of *C.citratus*

Organism	Zone of inhibition in mm		
	10 mg/ml	25 mg/ml	Std
<i>Staphylococcus aureus</i>	16±0.1	21±0.2	27±0.4
<i>Enterococcus faecalis</i>	14±0	23±0.6	25±0.14
<i>Escherichia coli</i>	14±0.6	18±0.9	26±0.1
<i>Klebsiella pneumoniae</i>	11±0.7	19±0.2	23±0
<i>Candida albicans</i>	17±1.0	22±0.01	21±0.01
Amp: Ampicillin 10mcg; Nx: Norfloxacin 10mcg ; Ap: Amphotericin 20mcg			

The hydro-alcoholic extract of *C. citratus* exhibited broad-spectrum antimicrobial activity (Table 2). Clear zones of inhibition were observed against all tested pathogens, consistent with the findings of Leite *et al.*, (2021). Gram-positive bacteria showed higher sensitivity, particularly *S. aureus* (21 ± 0.2 mm) and *E. faecalis* (23 ± 0.6 mm). Moderate activity against *E. coli*

and *K. pneumoniae* aligns with reported citral-induced membrane disruption mechanisms [24]. Activity against *Candida albicans* corroborates findings that lemongrass essential oil exhibits high antifungal activity [25] with varying potency at two different concentrations and results were given in **Table 2**.

Antioxidant Activity (DPPH Assay)**Fig. 6: DPPH assay for the whole plant of *Cymbopogon citratus*, Stapf**

The extract demonstrated significant free-radical scavenging activity, with maximal inhibition ($78.18 \pm 1.2\%$) at $10 \mu\text{g/mL}$ and IC_{50} of $39.37 \mu\text{g/mL}$. This potent antioxidant activity corresponds with phenolic and

flavonoid content and is comparable to results reported by [26 & 27] **Fig. 6.**

HPTLC Fingerprinting**Table 3: Rf values of the alcohol extract of *C.citratus* – Whole plant**

Extract	Track	Solvent system	UV-254nm	UV-366nm	Visible light
Alcohol	A	Toluene: Ethyl acetate: Formic acid (8.4:1.6:0.01)	0.99 - green 0.92 - green 0.81- dark green 0.55 - light green 0.19 - light green 0.13 - light green 0.09 - green 0.05 - light green	0.90- fluorescent red 0.86-red 0.81- red 0.79- blue 0.76- red 0.70- red 0.62- fluorescent red 0.50- red 0.40- yellowish green 0.37- light brown 0.34- bluish green 0.19- light red 0.15-light brown 0.10- light blue	0.93-yellowish green 0.85 - dark blue 0.77- dark grey 0.70 - light grey 0.65 - violet 0.58 - light black 0.50 - light grey 0.43 - light black 0.40 - light black 0.30 - light grey 0.15 - violet 0.06 - light grey 0.05 - light grey
	B		0.99- green 0.92- green 0.81- dark green 0.55- light green 0.19- light green 0.13- light green 0.09 - green 0.05- light green	0.90- fluorescent red 0.86-red 0.81- red 0.79- blue 0.76- red 0.70- red 0.62- fluorescent red 0.50- red 0.40- yellowish green 0.37- light brown 0.34- bluish green 0.19- light red 0.15-light brown 0.10- light blue	0.93-yellowish green 0.85- dark blue 0.77-dark grey 0.70- light grey 0.65-violet 0.58-light black 0.50-light grey 0.43-light black 0.40-light black 0.30-light grey 0.15-violet 0.06-light grey 0.05- light grey

Table 4: Rf values obtained after scanning at 254 nm in Absorption mode for track A

Peak	Start Position	Start Height	Max Position	Max Height	Max %	End Position	End Height	Area	Area %
1	0.00 Rf	131.9 AU	0.01 Rf	285.0 AU	37.70 %	0.03 Rf	0.0 AU	2074.7 AU	15.74 %
2	0.04 Rf	1.1 AU	0.05 Rf	18.2 AU	2.40 %	0.07 Rf	0.2 AU	184.0 AU	1.40 %
3	0.08 Rf	0.2 AU	0.10 Rf	61.7 AU	8.16 %	0.12 Rf	40.5 AU	1081.5 AU	8.20 %
4	0.12 Rf	41.0 AU	0.14 Rf	46.8 AU	6.19 %	0.18 Rf	2.8 AU	872.1 AU	6.62 %
5	0.18 Rf	3.0 AU	0.21 Rf	46.4 AU	6.13 %	0.26 Rf	0.6 AU	896.6 AU	6.80 %
6	0.64 Rf	4.6 AU	0.67 Rf	21.9 AU	2.90 %	0.70 Rf	13.8 AU	558.5 AU	4.24 %
7	0.70 Rf	14.1 AU	0.70 Rf	15.4 AU	2.04 %	0.75 Rf	3.8 AU	309.1 AU	2.35 %
8	0.92 Rf	0.1 AU	0.97 Rf	260.7 AU	34.48 %	1.00 Rf	70.3 AU	7204.3 AU	54.66 %

Table 5: Rf values obtained after scanning at 254nm in Absorption mode for track B

Peak	Start Position	Start Height	Max Position	Max Height	Max %	End Position	End Height	Area	Area %
1	0.00 Rf	206.7 AU	0.01 Rf	314.6 AU	35.97 %	0.03 Rf	0.0 AU	2250.5 AU	12.45 %
2	0.04 Rf	0.6 AU	0.05 Rf	17.1 AU	1.95 %	0.07 Rf	0.6 AU	178.2 AU	0.99 %
3	0.08 Rf	0.1 AU	0.10 Rf	55.6 AU	6.36 %	0.12 Rf	34.1 AU	1003.0 AU	5.55 %
4	0.13 Rf	34.4 AU	0.14 Rf	39.1 AU	4.47 %	0.16 Rf	8.3 AU	580.6 AU	3.21 %
5	0.19 Rf	8.3 AU	0.21 Rf	45.4 AU	5.19 %	0.25 Rf	5.8 AU	925.9 AU	5.12 %
6	0.39 Rf	2.4 AU	0.44 Rf	11.5 AU	1.31 %	0.46 Rf	3.8 AU	276.6 AU	1.53 %
7	0.62 Rf	5.7 AU	0.65 Rf	18.9 AU	2.16 %	0.68 Rf	14.1 AU	479.8 AU	2.65 %
8	0.68 Rf	14.1 AU	0.70 Rf	15.6 AU	1.78 %	0.75 Rf	0.8 AU	385.0 AU	2.13 %
9	0.90 Rf	0.1 AU	0.96 Rf	356.9 AU	40.81 %	1.00 Rf	20.6 AU	12004.1 AU	66.38 %

Table 6: R_f values obtained after scanning at 366 nm in Absorption mode for track A

Peak	Start Position	Start Height	Max Position	Max Height	Max %	End Position	End Height	Area	Area %
1	0.00 Rf	117.6 AU	0.01 Rf	273.2 AU	47.87 %	0.03 Rf	0.0 AU	1790.0 AU	20.93 %
2	0.04 Rf	0.3 AU	0.05 Rf	11.9 AU	2.08 %	0.07 Rf	0.1 AU	101.8 AU	1.19 %
3	0.08 Rf	0.3 AU	0.12 Rf	92.6 AU	16.21 %	0.16 Rf	9.7 AU	2034.0 AU	23.78 %
4	0.16 Rf	9.9 AU	0.17 Rf	10.7 AU	1.88 %	0.18 Rf	0.1 AU	104.0 AU	1.22 %
5	0.20 Rf	2.5 AU	0.22 Rf	10.7 AU	1.87 %	0.24 Rf	7.6 AU	185.1 AU	2.16 %
6	0.25 Rf	9.0 AU	0.27 Rf	21.0 AU	3.67 %	0.30 Rf	1.8 AU	431.0 AU	5.04 %
7	0.35 Rf	2.0 AU	0.39 Rf	17.4 AU	3.05 %	0.40 Rf	13.9 AU	330.3 AU	3.86 %
8	0.41 Rf	12.7 AU	0.46 Rf	67.1 AU	11.76 %	0.52 Rf	0.8 AU	1850.4 AU	21.63 %
9	0.55 Rf	2.7 AU	0.60 Rf	14.8 AU	2.59 %	0.61 Rf	14.7 AU	362.8 AU	4.24 %
10	0.62 Rf	14.4 AU	0.67 Rf	51.4 AU	9.01 %	0.70 Rf	1.3 AU	1364.2 AU	15.95 %

Table 7: Rf values obtained after scanning at 366 nm in Absorption mode for track B
50 μ

Peak	Start Position	Start Height	Max Position	Max Height	Max %	End Position	End Height	Area	Area %
1	0.01 Rf	225.5 AU	0.01 Rf	297.3 AU	53.61 %	0.03 Rf	0.0 AU	1734.7 AU	22.14 %
2	0.04 Rf	0.5 AU	0.05 Rf	11.4 AU	2.05 %	0.07 Rf	0.2 AU	98.0 AU	1.25 %
3	0.08 Rf	0.2 AU	0.11 Rf	85.3 AU	15.38 %	0.16 Rf	6.1 AU	1800.8 AU	22.98 %
4	0.22 Rf	10.6 AU	0.26 Rf	24.2 AU	4.36 %	0.30 Rf	2.0 AU	653.3 AU	8.34 %
5	0.34 Rf	1.7 AU	0.37 Rf	14.4 AU	2.60 %	0.39 Rf	11.9 AU	327.8 AU	4.18 %
6	0.40 Rf	12.1 AU	0.44 Rf	63.7 AU	11.49 %	0.50 Rf	0.1 AU	1682.2 AU	21.47 %
7	0.53 Rf	1.6 AU	0.58 Rf	15.9 AU	2.86 %	0.60 Rf	14.5 AU	441.6 AU	5.64 %
8	0.62 Rf	16.6 AU	0.65 Rf	42.4 AU	7.65 %	0.69 Rf	0.1 AU	1097.9 AU	14.01 %

Table 8: Rf values obtained after scanning at 366 nm in Fluorescence mode for track A

Peak	Start Position	Start Height	Max Position	Max Height	Max %	End Position	End Height	Area	Area %
1	0.01 Rf	225.5 AU	0.01 Rf	297.3 AU	53.61 %	0.03 Rf	0.0 AU	1734.7 AU	22.14 %
2	0.04 Rf	0.5 AU	0.05 Rf	11.4 AU	2.05 %	0.07 Rf	0.2 AU	98.0 AU	1.25 %
3	0.08 Rf	0.2 AU	0.11 Rf	85.3 AU	15.38 %	0.16 Rf	6.1 AU	1800.8 AU	22.98 %
4	0.22 Rf	10.6 AU	0.26 Rf	24.2 AU	4.36 %	0.30 Rf	2.0 AU	653.3 AU	8.34 %
5	0.34 Rf	1.7 AU	0.37 Rf	14.4 AU	2.60 %	0.39 Rf	11.9 AU	327.8 AU	4.18 %
6	0.40 Rf	12.1 AU	0.44 Rf	63.7 AU	11.49 %	0.50 Rf	0.1 AU	1682.2 AU	21.47 %
7	0.53 Rf	1.6 AU	0.58 Rf	15.9 AU	2.86 %	0.60 Rf	14.5 AU	441.6 AU	5.64 %
8	0.62 Rf	16.6 AU	0.65 Rf	42.4 AU	7.65 %	0.69 Rf	0.1 AU	1097.9 AU	14.01 %

Table 9: Rf values obtained after scanning at 366 nm in Fluorescence mode for track B

Peak	Start Position	Start Height	Max Position	Max Height	Max %	End Position	End Height	Area	Area %
1	0.00 Rf	0.0 AU	0.02 Rf	102.3 AU	11.95 %	0.08 Rf	55.8 AU	3273.7 AU	15.76 %
2	0.08 Rf	56.1 AU	0.11 Rf	225.8 AU	26.39 %	0.14 Rf	53.6 AU	4466.2 AU	21.49 %
3	0.16 Rf	51.2 AU	0.17 Rf	52.4 AU	6.13 %	0.19 Rf	42.3 AU	1021.1 AU	4.91 %
4	0.19 Rf	42.4 AU	0.21 Rf	59.6 AU	6.97 %	0.24 Rf	40.0 AU	1402.9 AU	6.75 %
5	0.24 Rf	40.1 AU	0.26 Rf	68.3 AU	7.98 %	0.27 Rf	42.1 AU	977.9 AU	4.71 %
6	0.34 Rf	40.9 AU	0.40 Rf	64.6 AU	7.55 %	0.44 Rf	50.3 AU	3503.8 AU	16.86 %
7	0.47 Rf	44.5 AU	0.48 Rf	115.4 AU	13.49 %	0.50 Rf	23.2 AU	1054.9 AU	5.08 %
8	0.53 Rf	23.5 AU	0.59 Rf	34.4 AU	4.02 %	0.61 Rf	29.5 AU	1704.6 AU	8.20 %
9	0.62 Rf	29.6 AU	0.66 Rf	70.0 AU	8.18 %	0.69 Rf	13.0 AU	1969.2 AU	9.48 %
10	0.70 Rf	11.3 AU	0.73 Rf	27.6 AU	3.22 %	0.79 Rf	5.0 AU	792.5 AU	3.81 %
11	0.87 Rf	1.0 AU	0.90 Rf	16.9 AU	1.97 %	0.93 Rf	0.3 AU	345.2 AU	1.66 %
12	0.94 Rf	0.1 AU	0.96 Rf	18.5 AU	2.16 %	0.98 Rf	0.3 AU	266.3 AU	1.28 %

Table 10: Rf values obtained after scanning at 520 nm in absorption mode for track A

Peak	Start Position	Start Height	Max Position	Max Height	Max %	End Position	End Height	Area	Area %
1	0.00 Rf	31.7 AU	0.01 Rf	212.7 AU	41.81 %	0.03 Rf	0.0 AU	1395.5 AU	16.31 %
2	0.05 Rf	0.1 AU	0.06 Rf	24.5 AU	4.81 %	0.08 Rf	0.0 AU	197.1 AU	2.30 %
3	0.09 Rf	0.5 AU	0.10 Rf	10.9 AU	2.15 %	0.14 Rf	4.4 AU	209.4 AU	2.45 %
4	0.28 Rf	4.5 AU	0.34 Rf	40.8 AU	8.02 %	0.38 Rf	3.6 AU	1245.9 AU	14.56 %
5	0.42 Rf	1.6 AU	0.46 Rf	14.2 AU	2.78 %	0.49 Rf	4.8 AU	367.0 AU	4.29 %
6	0.54 Rf	0.0 AU	0.59 Rf	50.2 AU	9.86 %	0.64 Rf	1.6 AU	1416.3 AU	16.56 %
7	0.64 Rf	1.9 AU	0.67 Rf	25.5 AU	5.01 %	0.70 Rf	0.0 AU	565.7 AU	6.61 %
8	0.70 Rf	0.1 AU	0.75 Rf	60.6 AU	11.91 %	0.78 Rf	9.8 AU	1454.9 AU	17.01 %
9	0.84 Rf	11.4 AU	0.89 Rf	37.7 AU	7.40 %	0.92 Rf	0.3 AU	1084.8 AU	12.68 %
10	0.94 Rf	0.0 AU	0.98 Rf	31.8 AU	6.25 %	0.99 Rf	19.4 AU	618.4 AU	7.23 %

Table 11: Rf values obtained after scanning at 520 nm in absorption mode for track B

Peak	Start Position	Start Height	Max Position	Max Height	Max %	End Position	End Height	Area	Area %
1	0.00 Rf	12.6 AU	0.01 Rf	222.1 AU	40.86 %	0.03 Rf	0.0 AU	1536.7 AU	15.91 %
2	0.03 Rf	0.0 AU	0.06 Rf	21.8 AU	4.01 %	0.08 Rf	0.7 AU	194.5 AU	2.01 %
3	0.27 Rf	2.3 AU	0.32 Rf	38.2 AU	7.02 %	0.37 Rf	1.3 AU	1110.7 AU	11.50 %
4	0.41 Rf	0.0 AU	0.44 Rf	13.3 AU	2.45 %	0.48 Rf	2.7 AU	286.7 AU	2.97 %
5	0.53 Rf	0.2 AU	0.58 Rf	48.1 AU	8.84 %	0.62 Rf	4.2 AU	1432.6 AU	14.83 %
6	0.62 Rf	4.3 AU	0.65 Rf	26.2 AU	4.82 %	0.69 Rf	0.2 AU	604.8 AU	6.26 %
7	0.69 Rf	0.1 AU	0.73 Rf	58.4 AU	10.74 %	0.77 Rf	11.4 AU	1514.2 AU	15.68 %
8	0.78 Rf	15.4 AU	0.80 Rf	25.0 AU	4.59 %	0.82 Rf	7.2 AU	462.8 AU	4.79 %
9	0.83 Rf	8.0 AU	0.87 Rf	35.3 AU	6.49 %	0.91 Rf	0.3 AU	1082.5 AU	11.21 %
10	0.92 Rf	0.0 AU	0.98 Rf	55.2 AU	10.16 %	0.99 Rf	24.0 AU	1434.4 AU	14.85 %

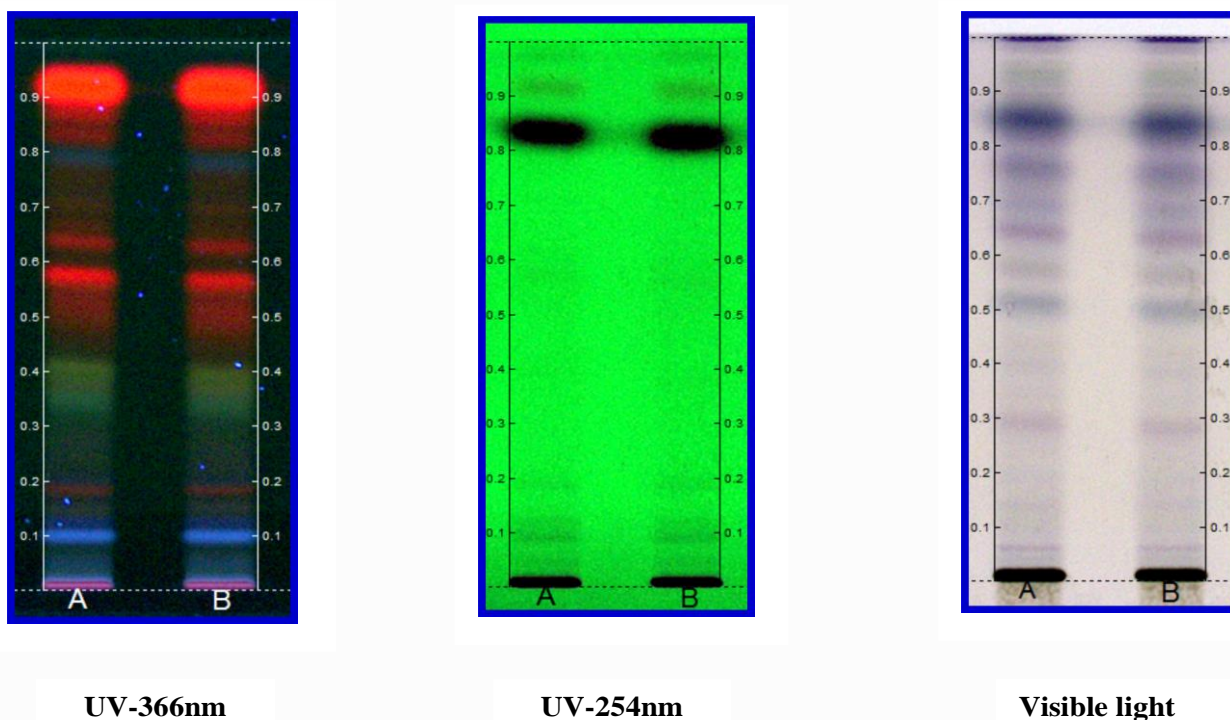


Fig. 7 Photo documentation of HPTLC Fingerprints of *C.citratus* in alcohol extract

HPTLC

The HPTLC chromatographic fingerprinting of crude alcoholic extract of the whole plant of *C.citratus* was developed under the chromatographic conditions described above. **Fig. 7** shows the HPTLC fingerprinting (alcoholic extract) of the whole plant of *C.citratus*. **Table 3** gives the R_f values of two similar tracks with the same concentration of the alcohol extract of the plant material. **Table 4** shows the R_f values obtained after scanned at 254nm in Absorption mode for track A reveals 8 spots at R_f 0.92, 0.70, 0.64, 0.18, 0.12, 0.08, 0.04 and 0.01. **Table 5** shows the R_f values obtained after scanning at 254nm in Absorption mode for track B reveals 9 spots at R_f 0.90, 0.68, 0.62, 0.39, 0.19, 0.13, 0.08, 0.04 and 0.01. **Table 6** shows the R_f values obtained after scanning at 366nm in Absorption mode for track A reveals 10 spots at R_f 0.62, 0.55, 0.41, 0.35, 0.25, 0.20, 0.16, 0.08, 0.04 and 0.01. **Table 7** shows the R_f values obtained after scanning at 366nm in Absorption mode for track B reveals 8 spots at R_f 0.62, 0.53, 0.40, 0.34, 0.22, 0.08, 0.04 and 0.01. **Table 8** shows the R_f values obtained after scanning at 366nm in fluorescence mode for track A reveals 10 spots at R_f 0.95, 0.88, 0.71, 0.60, 0.46, 0.35, 0.20, 0.17, 0.08 and 0.01. **Table 9** shows the R_f values obtained after scanning at 366nm in fluorescence mode for track B reveals 12 spots at R_f 0.94, 0.87, 0.70, 0.62, 0.53, 0.47, 0.34, 0.24, 0.19, 0.16, 0.08 and 0.01. **Table 10** shows the R_f values obtained after scanning at 520nm in absorption mode for track A reveals 10 spots at R_f 0.94, 0.84, 0.70, 0.64, 0.54, 0.42, 0.28, 0.09, 0.05 and 0.01. **Table 11** shows the R_f values obtained after scanning at 520 nm in absorption mode for track B reveals 10 spots at R_f 0.92, 0.83, 0.78, 0.69, 0.62,

0.53, 0.41, 0.27, 0.03 and 0.01. Both 254nm and 366nm Densitometric scan data shows three significant spots at R_f values 0.08, 0.04 and 0.01 in absorption mode. Hence this study gives us the qualitative identification of various phytoactive constituents contain in the alcohol extract of the whole plant of *C.citratus* and will be used as the phytochemical fingerprint standard for quality control studies and also to identify the adulterants added to the drug.

DISCUSSION

Proper identification and quality assessment of medicinal plants are essential for ensuring their authenticity, safety, and efficacy. According to the World Health Organization (WHO), macroscopic and microscopic examinations form the first and most critical steps in determining the identity and purity of plant materials and should be completed before any chemical or biological analyses are undertaken [28]. In the present study, the detailed pharmacognostic evaluation of *Cymbopogon citratus* aligns with earlier reports that highlighted key anatomical features of *C. citratus* and *C. schoenanthus*, including vascular bundles surrounded by sclerenchymatous sheaths and 3–4 layers of sclerenchyma at the bundle base typical characteristics of monocotyledonous grasses [29 & 30]. These diagnostic anatomical markers observed in our study further validate the taxonomic identity of the plant.

Previous pharmacognostic investigations of *C. citratus* have documented leaf constants, microscopical traits, preliminary phytochemical profiles, and

chromatographic fingerprints [31]. Our findings corroborate these reports and additionally highlight features such as dumb-bell-shaped silica bodies, bulliform cells, annular vessels, and specific trichome types, strengthening the diagnostic criteria for quality control. Such data are vital, especially considering the increasing global use of herbal raw materials and the frequent issues of adulteration and substitution in commercial herbal markets [32].

The antimicrobial activity observed in this study is consistent with earlier studies demonstrating strong inhibitory effects of *C. citratus* extracts against both Gram-positive and Gram-negative bacteria, particularly *Staphylococcus aureus* [33 & 34]. The antimicrobial properties are largely attributed to citral (geranial and neral), myrcene, citronellal, and other minor constituents such as chryslandicin derivatives and aspilactonol B [35 & 36]. The close agreement between our results and previous studies reinforces the therapeutic relevance of *C. citratus* in treating microbial infections.

Similarly, the antioxidant activity recorded in our study supports the long-standing traditional use of lemongrass as a therapeutic herb. Flavonoids and phenolic acids—major constituents of *C. citratus* are known for free radical scavenging, hydrogen-donating, and reducing capacities [37 & 38]. These molecules help counter oxidative stress, which plays a significant role in the pathogenesis of various chronic and inflammatory disorders. The high antioxidant potential observed in our study aligns with reports that link the bioactivities of *C. citratus* to compounds such as quercetin, luteolin, kaempferol, apigenin, and isoorientin-2'-O-rhamnoside [39]. Identifying these constituents provides strong scientific support for its ethnomedicinal claims. The HPTLC fingerprint developed in this study offers an important tool for the rapid authentication and standardization of *C. citratus*. HPTLC is recognized as a cost-effective, high-throughput, and reproducible method widely used for herbal drug analysis [40 & 41]. The presence of consistent Rf values and the detection of multiple phytochemical classes across different wavelengths confirm the chemical complexity and authenticity of the plant material. This fingerprint can serve as a reference standard for ensuring quality across commercial batches.

CONCLUSION

Pharmacognosy plays a pivotal role in the discovery and scientific evaluation of bioactive compounds derived from medicinal plants. Although a large number of species within the Poaceae family remain insufficiently explored, the present study offers the first comprehensive pharmacognostic profile of *Cymbopogon citratus* (Stapf.), contributing valuable baseline data for its accurate identification, authentication, and quality control. The whole-plant extract demonstrated a high abundance of phenolic compounds such as phenolic acids, O- and C-glycosyl

flavones, and tannins which accounted for its strong antioxidant and notable antibacterial activities. The DPPH assay further confirmed the plant's free radical scavenging potential. The HPTLC fingerprint generated in this study provides a reliable chemical profile and serves as an essential tool for standardization of *C. citratus*, enabling rapid detection of key phytochemicals and supporting its quality assurance in herbal formulations. The visualized bands and consistent Rf values confirm the presence of pharmacologically important constituents, strengthening the scientific basis for its therapeutic applications.

While the study successfully establishes fundamental pharmacognostic and bioactivity data, certain limitations remain. Quantitative estimation of specific marker compounds was not performed, and antimicrobial evaluation was restricted to disc diffusion assays. Additionally, potential variations in phytochemical composition due to environmental or seasonal factors were not assessed. These limitations highlight the need for further investigation to deepen the understanding of *C. citratus*. Future research should focus on quantifying major bioactive constituents using advanced chromatographic techniques, performing MIC/MBC assays for more precise antimicrobial characterization, and exploring metabolomic diversity across different growing conditions. Bioactivity-guided fractionation and in-vitro mechanistic studies may also help identify the most potent therapeutic components. Overall, this study provides a strong foundation for further characterization of *C. citratus* and its potential development into scientifically validated herbal therapeutics.

Acknowledgments

The authors are thankful to the Director General, CCRUM, Ministry of AYUSH, Government of India, New Delhi for financial support for carrying out this research work.

REFERENCES

1. World Health Organization. (2011). *Quality control methods for herbal materials* (Updated ed.). WHO Press.
2. Payyappallimana, U., & Patrick, D. (2020). Traditional medicine and primary health care in Africa: Relevant issues and challenges. *Frontiers in Pharmacology*, 11, 548.
3. Ghorbani, A., & Esmaeilzadeh, M. (2017). Pharmacological properties of medicinal plants: A review. *Research in Pharmaceutical Sciences*, 12(3), 173–181.
4. Raskin, I., & Ripoll, C. (2024). The dawn of botanical therapeutics: Historical, ethnopharmacological, and modern perspectives. *Nature Reviews Drug Discovery*, 23, 85–102.
5. Wink, M. (2020). Potential molecular modes of action of medicinal and aromatic plant metabolites: A review. *Plants*, 9(9), 1127.

6. Sharma, P., Verma, S., & Rekha, R. (2021). Morphological diversity and taxonomic significance in Poaceae. *Journal of Plant Taxonomy and Systematics*, 27(2), 145–156. <https://doi.org/10.1007/jpts.2021.0156>
7. Bashir, T., Hassan, N., & Dar, R. (2022). Global species distribution and chemotypic variability of the genus *Cymbopogon*: A comprehensive review. *Industrial Crops and Products*, 178, 114603. <https://doi.org/10.1016/j.indcrop.2022.114603>
8. Almarzuqi, M., Balogun, T., Al-Hashimi, A., & Rajhi, A. (2023). Chemical profiling and biological activities of *Cymbopogon citratus* essential oil: A modern perspective. *Plants*, 12(3), 512. <https://doi.org/10.3390/plants12030512>
9. Nunes, C., Coimbra, M. A., & Santos, J. A. (2020). Bioactive secondary metabolites in medicinal and aromatic plants: A review on antioxidant applications. *Phytochemistry Reviews*, 19(5), 1241–1265. <https://doi.org/10.1007/s11101-020-09693-2>
10. De Carvalho, A. P., Oliveira, J. S., & Almeida, P. R. (2023). Agronomic performance and essential oil yield of *Cymbopogon citratus* under varying soil and light conditions. *Agronomy Journal*, 115(1), 245–256. <https://doi.org/10.1002/agj2.21345>
11. Akhgari, A., Farhadi, F., & Dolatabadi, S. (2020). Industrial, cosmetic, and aromatic applications of *Cymbopogon* species essential oils: An updated review. *Journal of Essential Oil Research*, 32(4), 289–302. <https://doi.org/10.1080/10412905.2020.1743531>
12. Moghadamtousi, S. Z., Karimian, H., & Abdulla, M. A. (2021). Ethnopharmacological uses and medicinal potential of *Cymbopogon citratus* (DC.) Stapf: A review. *Frontiers in Pharmacology*, 12, 637802. <https://doi.org/10.3389/fphar.2021.637802>
13. Nagarajan, R., & Rajendran, K. (2022). Pharmacological and therapeutic potential of *Cymbopogon citratus*: A systematic review. *Journal of Ethnopharmacology*, 285, 114987. <https://doi.org/10.1016/j.jep.2021.114987>
14. Singh, S., & Patel, R. (2019). Ayurvedic perspectives and traditional uses of *Cymbopogon citratus*. *AYU*, 40(3), 160–166. https://doi.org/10.4103/ayu.ayu_26_19
15. Leite, M. C., de Brito, A. S., & de Sousa, J. P. (2021). Citral-rich essential oils as antifungal agents against *Candida* species: Mechanistic insights and therapeutic potential. *Journal of Applied Microbiology*, 130(1), 245–256. <https://doi.org/10.1111/jam.14870>
16. Chowdhury, A. R., Hossain, M. A., & Haque, M. E. (2020). Therapeutic properties of *Cymbopogon citratus*: A comprehensive review on phytochemistry and pharmacology. *Biomedicine & Pharmacotherapy*, 128, 110318. <https://doi.org/10.1016/j.biopha.2020.110318>
17. Rodrigues, J. C., Silva, L. L., & Moreira, D. L. (2019). Antimalarial properties of citral and related monoterpenes against *Plasmodium falciparum*. *Malaria Journal*, 18, 326. <https://doi.org/10.1186/s12936-019-2974-5>
18. Bozic, D., Djordjevic, L., & Brkic, D. (2022). Essential oil constituents with antimalarial potential: In vitro evaluation of *Cymbopogon citratus* compounds. *Pharmaceutical Biology*, 60(1), 1234–1242. <https://doi.org/10.1080/13880209.2022.2098433>
19. Evans, W. C. (2014). *Trease and Evans pharmacognosy* (15th ed.). Elsevier.
20. Ranade, S. S., & Thiagarajan, P. (2015). Lemon grass. *International Journal of Pharmaceutical Sciences Review and Research*, 35(2), 162–167.
21. World Health Organization. (2011). *Quality control of herbal medicine*. WHO.
22. Clinical and Laboratory Standards Institute. (2010). *Performance standards for antimicrobial susceptibility testing*. CLSI.
23. Brand-Williams, W., Cuvelier, M. E., & Berset, C. L. (1995). Use of a free radical method to evaluate antioxidant activity. *LWT – Food Science and Technology*, 28(1), 25–30.
24. Chowdhury, A. R., Hossain, M. A., & Haque, M. E. (2020). Pharmacology of *Cymbopogon citratus*. *Biomedicine & Pharmacotherapy*, 128, 110318. <https://doi.org/10.1016/j.biopha.2020.110318>
25. Leite, M. C., de Brito, A. S., & de Sousa, J. P. (2021). Citral-rich oils as antifungal agents. *Journal of Applied Microbiology*, 130(1), 245–256. <https://doi.org/10.1111/jam.14870>
26. Nunes, C., Coimbra, M. A., & Santos, J. A. (2020). Bioactive secondary metabolites in medicinal plants. *Phytochemistry Reviews*, 19, 1241–1265. <https://doi.org/10.1007/s11101-020-09693-2>
27. Akhgari, A., Farhadi, F., & Dolatabadi, S. (2020). Industrial and pharmacological applications of *Cymbopogon* essential oils. *Journal of Essential Oil Research*, 32(4), 289–302. <https://doi.org/10.1080/10412905.2020.1743531>
28. World Health Organization. (2019). *WHO global report on traditional and complementary medicine 2019*. WHO.
29. Sharma, P., & Kumar, N. (2020). Comparative pharmacognostic and microscopic evaluation of *Cymbopogon citratus* and *Cymbopogon schoenanthus*. *Journal of Applied Research on Medicinal and Aromatic Plants*, 19, 100274. <https://doi.org/10.1016/j.jarmap.2020.100274>
30. Adebisi, A., Oyediji, O. A., Olorunnisola, O. S., & Adegbola, P. (2019). Pharmacognostic, anatomical and physicochemical profiling of *Cymbopogon citratus* leaves. *BMC Complementary and Alternative Medicine*, 19, 350. <https://doi.org/10.1186/s12906-019-2764-2>
31. Ghosh, S., & Mandal, A. (2021). Pharmacognostical and HPTLC investigation of *Cymbopogon citratus* leaves for authentication and quality control. *Industrial Crops and Products*, 171, 113944. <https://doi.org/10.1016/j.indcrop.2021.113944>

32. Joshi, R. K. (2023). Adulteration and substitution in herbal drugs: Current challenges and analytical perspectives. *Journal of Herbal Medicine*, 36, 100634. <https://doi.org/10.1016/j.hermed.2023.100634>
33. Olorundare, O. E., Adebayo, O. O., Ahmed, A. S., & Majolagbe, O. N. (2021). Antibacterial efficacy of *Cymbopogon citratus* extracts against clinical strains of *Staphylococcus aureus* and *Escherichia coli*. *South African Journal of Botany*, 139, 406–413. <https://doi.org/10.1016/j.sajb.2021.03.033>
34. Al-Mariri, A., & Safi, M. (2020). In vitro antibacterial activity of essential oils from *Cymbopogon citratus* against multi-drug resistant pathogens. *Microbial Pathogenesis*, 149, 104546. <https://doi.org/10.1016/j.micpath.2020.104546>
35. Haque, M. A., Rahman, M. M., & Hossain, M. A. (2022). Chemical profiling and antimicrobial potential of *Cymbopogon citratus* essential oil: The role of citral and minor components. *Chemico-Biological Interactions*, 363, 110029. <https://doi.org/10.1016/j.cbi.2022.110029>
36. Lv, F., Liang, H., Yuan, Q., & Li, C. (2021). Mechanism of antibacterial activity of citral on bacterial cell membranes. *Food Control*, 127, 108124. <https://doi.org/10.1016/j.foodcont.2021.108124>
37. Mathew, A., Analiparambil Ravindran, R., Vazhanthodi, A. R., Valiyaparambil Sivadasan, B., Ovungal, S., Madathilpadi Subrahmanian, S., Chittadimangalath, P., & Anthyalam Parambil, A. (2022). Microwave-assisted greener synthesis of silver nanoparticles using *Entada rheedii* leaf extract and investigation of its anticancer and antimicrobial properties. *International Journal of Nano Dimension*, 13(3), 329–334.
38. Macedo, J. D., Copatti, C. E., Costa, E. V., da Silva, F. M., Dutra, L. M., Santos, V. L., Almeida, J. R., Tavares-Dias, M., & Melo, J. F. (2023). Effects of *Citrus limon* extract on growth performance and immunity in striped catfish (*Pangasius hypophthalmus*). *Aquaculture International*, 31(2), 719–738.
39. Islam, M. T., Ali, E. S., Uddin, S. J., Islam, M. A., Shaw, S., Khan, I. N., & Mubarak, M. S. (2020). Chemical constituents, flavonoid profiling, and antioxidant properties of *Cymbopogon citratus*. *Arabian Journal of Chemistry*, 13(1), 174–187. <https://doi.org/10.1016/j.arabjc.2017.04.004>
40. Sherma, J., & Rabel, F. (2019). High-performance thin-layer chromatography for the analysis of medicinal plants. *Journal of Liquid Chromatography & Related Technologies*, 42(13–14), 467–489. <https://doi.org/10.1080/10826076.2019.1640767>
41. Sasidharan, S., Chen, Y., Saravanan, D., & Sundram, K. (2022). Application of HPTLC for authentication and standardization of medicinal plants: Advances and challenges. *Journal of Pharmaceutical and Biomedical Analysis*, 209, 114532. <https://doi.org/10.1016/j.jpba.2021.114532>